Desalination and Water Treatment
www.deswater.com
doi: 10.5004/dwt.2019.24354

162 (2019) 303–312
September

Polymeric metal complex-derived nitrogen-doped carbon-encapsulated α-Fe_2O_3 (NCF) nanocomposites as highly efficient adsorbent for the removal of Cd^{2+} ion from aqueous medium

Saad M. Alshehri[a], Mu. Naushad[a,*], Tansir Ahamad[a], Norah Alhokbany[a], Tokeer Ahmad[b], Jahangeer Ahmed[a,*]

[a]*King Saud University, Department of Chemistry, College of Science, Riyadh 11451, Saudi Arabia, emails: mnaushad@ksu.edu.sa (M. Naushad), jahmed@ksu.edu.sa (J. Ahmed)*
[b]*Nanochemistry Laboratory, Department of Chemistry, Jamia Millia Islamia, New Delhi 110025, India*

Received 25 February 2019; Accepted 2 May 2019

ABSTRACT

Polymeric precursor procedure was employed in the synthesis of nitrogen-doped carbon-encapsulated α-Fe_2O_3 (NCF) nanocomposite (NC) at 325°C. Electron microscopic studies confirm the formation of encapsulated α-Fe_2O_3 nanoparticles (~20 nm) in nitrogen-doped carbon matrix. X-ray diffraction, Fourier-transform infrared spectroscopy, energy dispersive, and X-ray photoelectron spectroscopy studies were used to confirm the presence of nitrogen containing carbon in NCF-NCs. The NCF-NC was used as an efficient adsorbent in the removal of Cd(II) ion from aqueous medium. Batch adsorption studies were performed to optimize the various adsorption parameters such as contact time (2–240 min), pH (2–8), temperature (25°C–45°C) and initial concentration of Cd^{2+} ion (20–100 mg/L). The optimum pH and time for the adsorption of Cd^{2+} were 6.0 and 120 min, respectively. The course of adsorption was described by Langmuir and Freundlich isotherms and better correlation coefficient was achieved for Langmuir model. The maximum adsorption capacity at 25°C was 208.3 mg/g by using the Langmuir equation.

Keywords: Nitrogen-doped carbon; Nanocomposites; Adsorption; Toxic metal; Cd^{2+}

1. Introduction

Potential applications of environment, removal of toxic substances from water, have engaged the researchers from the last few decades. The polluted water causes undesirable effect on aquatic and non-aquatic life [1–3]. Advanced nanotechnology provides feasible solutions to overcome the contaminated water problem worldwide [4]. Various techniques have been employed for the removal of toxic substances from polluted water such as ion-exchange [5,6], precipitation [7], filtration [8], photolysis [9,10], reverse osmosis [11], and adsorption [12–14]. The adsorption process has been considered as one of the best widely used methods in wastewater treatment due to low cost and high efficiency. Various kinds of adsorbents or catalysts such as polymers [15,16], fly ash [17], nanocomposites [18,19], bio-composites [20], metal organic frameworks [21], hydrogel [22], ferrite [23,24], functionalized core@shell [25], and functionalized porous silica [26] are used in the removal of inorganic and organic pollutants (i.e., heavy metals and colored dyes) from water. These heavy metal ions (Cr^{3+}, Cd^{2+}, Hg^{2+}, Pb^{2+} As^{5+}, etc.) are known as inorganic pollutants, which pose serious health threats to human being [27].

Apart from the above adsorbents, activated carbon (AC) was also used as an adsorbent in the adsorption of heavy metal ions [28–30]. High surface area, porous nature and

* Corresponding authors.

greatly active surface of the materials significantly enhance the properties of AC adsorbents. Though, the activated carbon (AC) as an adsorbent shows low adsorption capacities and selectivity of heavy metal ions. Therefore, selectivity and adsorption capacity of AC could be improved by the introduction of heteroatoms such as nitrogen (N) in graphite carbon. N-atom in carbon fundamentally exists as pyrrole and pyridine, which provides un-paired electrons for the coordination with the heavy metal ions to promote the elimination of the heavy metal ions from polluted water [31]. Mn-doped alpha-Fe_2O_3 [32], Fe_2O_3–Al_2O_3 [33,34], Fe_2O_3@AlO(OH) [35], IOARM [36], and gamma Fe_2O_3/carbon [37] nanoparticles were used as the adsorbents for the removal of heavy metals such as arsenic, chromium, lead, mercury, etc. from aqueous. Previously, we have developed metal tungstate and chromate nanostructured materials as efficient photo-catalysts for the degradation of organic pollutants from water [9,10,38]. In this paper, we report low-cost synthesis of NCF-NC at 325°C as an efficient adsorbent for the removal of Cd^{2+} ion from water. The structural, surface and morphological studies of NCF-NC were examined in details. To find the economical ways of the preparation of highly efficient adsorbents materials also have some fundamental concerns in this area. The main purpose of current study is to gauge the probability to develop an eco-friendly and low-cost alternative adsorbents with high removal efficiency for the removal of highly toxic Cd^{2+} from aqueous medium.

2. Experimental

A typical polymeric metal complex has been used for the synthesis of NCF-NC. 0.1 mole of urea was dissolved in 10 mL of DI water followed by the addition of 0.2 mole of formaldehyde. The pH of the resulting solution (~12) was adjusted by the addition of 2 mL of 0.1 M NaOH solution. The above solution was kept for 15 min at constant stirring (system A). Parallel, 0.005 moles of each, $FeCl_2{\cdot}4H_2O$ and $FeCl_3$, were dissolved in 100 mL of DI water (system B). Thereafter, system B was poured to system A and kept at 80°C for 45 min on continuous magnetic stirring. The brown colored precipitates appeared. These precipitates were filtered by vacuum filtration process and then dried in oven at 80°C for 24 h. The resulting powder at 80°C was used as a polymeric precursor in the synthesis of NCF-NC at 325°C for 3 h. Structural characterization of the precursor and nanocomposites was investigated on powder X-ray diffraction (Rigaku MiniFlex, Ni-filtered-CuKα radiation, USA), and Fourier-transform infrared spectroscopy (FTIR) (Bruker TENSOR-27 Spectrometer). Surface morphology of nanocomposites was recorded on field emission-transmission electron microscopy (FE-TEM; JEOL, JSM-2100F, USA) at 200 kV. X-ray photoelectron spectroscopy (XPS) of NCF-NCs was done on a Kratos Axis Ultra-DLD electron-spectrometer (PHI, PHI5300). The energy calibration and smoothing of the XPS analysis were done as also reported elsewhere [39,40]. The adsorption ability of NCF nanocomposite for the removal of Cd^{2+} was studied by batch method. 50 mg of NCF material was shaken with 100 mL of Cd^{2+} solution of known concentration in the Erlenmeyer's flasks for different time until the equilibration was achieved. The initial pH of the solution was adjusted by using 1.0 M HCl/NaOH solutions. After equilibration time, the solution was filtered and the filtrate was analyzed by AAS to measure the residual concentration of Cd^{2+} in the solution phase. All of the experiments were conducted in triplicate and the average values were used for data analysis. The equilibrium adsorption capacity (q, mg/g) was calculated by the following equation:

$$q_e = \frac{V(C_0 - C_e)}{m} \tag{1}$$

To perform the adsorption kinetics experiments, 50 mg of NCF-NC was mixed with 250 mL of Cd(II) ion solution of known concentration at a pH of 6. Subsequently, the above mixture was shaken at room temperature. The material samples were pipetted out at a fixed time, filtered using 0.22 μm filter and analyzed to find the residual concentration of Cd^{2+} in solution phase. The adsorption isotherms experiments were carried out by taking 50 mg of NCF with 100 mL of Cd^{2+} solution with varying initial concentrations (20–150 mg L^{-1}) and constant pH of 6. The flasks were shaken at three different temperatures 25°C, 35°C and 40°C. The materials were withdrawn after equilibration time followed by the analysis using the above mentioned method.

3. Results and discussion

Thermogravimetric analysis (TGA) of synthesized polymeric precursor of NCF-NC is shown in Fig. 1a. TGA shows a gradual weight loss from 100°C for NCF-NC. The weight loss (~76%) occurs from 100°C to 600°C, which corresponds to loss of water, carbon dioxide and nitrogenous molecules. Differential scanning calorimetry studies show an endotherm at ~275°C corresponding to the first weight loss of polymeric precursor. This is noticeable that decomposition of precursor in the presence of air occurs at an exothermic transition due to molecular carbon dioxide formation, but thermal decomposition of carbonyl substance in inert atmosphere follow an endothermic process as also reported elsewhere [41,42]. An exothermic peak is observed at ~750°C which could be attributed to the phase transition of alpha Fe_2O_3. PXRD studies of synthesized polymeric precursor show amorphous nature (Fig. 1b, blue colored pattern). PXRD patterns of annealed polymeric precursor (~325°C) reveal the formation of α-Fe_2O_3 nanoparticles in nitrogen doped carbon matrix. The diffraction pattern is perfectly matched with hexagonal crystal system of α-Fe_2O_3 (JCPDS # 86-0550). The noisy background with the occurrence of a small peak at ~26.40 indicates the occurrence of nitrogen containing carbon of the resulting materials. Pure α-Fe_2O_3 nanoparticles were also prepared at 600°C for 6 h and the PXRD patterns indexed on the basis of hexagonal system and no other phases were obtained. Energy dispersive studies (EDS) of NCF-NC were considered for elemental analysis (Fig. 1c). Note that EDS was equipped with FE-TEM. Energy dispersive study of NCF-NC shows presence of Fe and carbon with weak and strong intense lines respectively. It also shows the presence of nitrogen (NKα) at 0.392 keV. Weak intense lines of Fe are appeared due to the encapsulation of the nanoparticles by the mesoporous carbon, which is confirmed by the electron microscopic studies. The appearance of copper line in EDS spectrum is due to the presence of copper based TEM grid. Fig. 1d represents

the FTIR spectra of the synthesized polymeric precursor and NCF-NC. The FTIR spectrum of the precursor confirms the characteristic FTIR bands of Fe-O bands, which appear at lower wavenumber regions (470 and 548 cm^{-1}). The absorption bands in the region from 650 to 950 cm^{-1} could be attributed to nitrogen-containing substances. The FTIR peaks in the region of 1,040–1,380 cm^{-1} can be ascribed to the vibrations of C–H, C–N and C=C. The FTIR bands at ~1640, and ~2,840–2,960 cm^{-1} belong to the stretching vibrations of C=C and C–H bands, respectively. The peak at ~3,350 cm^{-1} is ascribed to the adsorbed H_2O molecule (H–O–H) in powder samples [43,44]. The broad FTIR band in the range from 1,000 to 1,700 cm^{-1} is related to the presence of nitrogen and carbon containing functional groups at 300°C as also shown in red colored FTIR spectrum of NCF-NC. FTIR spectrum also confirms the formation of pure α-Fe_2O_3 nanoparticles as shown with blue colored line in Fig. 1d. Field emission-transmission electron microscopy (FE-TEM) and scanning electron microscopy (FE-SEM) show the surface morphology and particle size analysis. Figs. 2a and b show the FESEM images of NCF-NC and pure α-Fe_2O_3 nanoparticles. FE-TEM studies clearly demonstrate that the α-Fe_2O_3 nanoparticles are encapsulated by nitrogen doped carbon (Fig. 2c). The average particle size is found to be ~20 nm (Fig. 2d). High resolution FE-TEM image gives the d-spacing of 2.94 Å, which matches with <110> plane of hexagonal structure of α-Fe_2O_3 (Fig. 2e). FE-TEM images of pure α-Fe_2O_3 show the agglomeration of nanoparticles, which could be due to high annealed temperature (i.e., 600°C) for 6 h (Fig. 2f). The BET surface area of NCF-NC (~105 m^2/g) was found to be five times higher than that of pure α-Fe_2O_3 (~20 m^2/g).

Fig. 3a shows the effect of contact time on the adsorption of Cd^{2+} using NCF-NC. The uptake of Cd^{2+} was increased with increasing the temperature. The adsorption was only 36% at 5 min which was reached up to 87% at 120 min. But, there was no change noted after 120 min, so 120 min was taken as an equilibration time. It was also noticed that adsorption was faster at the initial stages which might be due to the presence of large number of vacant sites on the surface of NCF in the starting [45]. The effect of solution pH plays an important role for the removal of any metal ion from aqueous medium [21]. In our study, the adsorption of Cd^{2+} onto NCF was low in the acidic medium which was due to the higher concentration and mobility of H^+ ions present in the

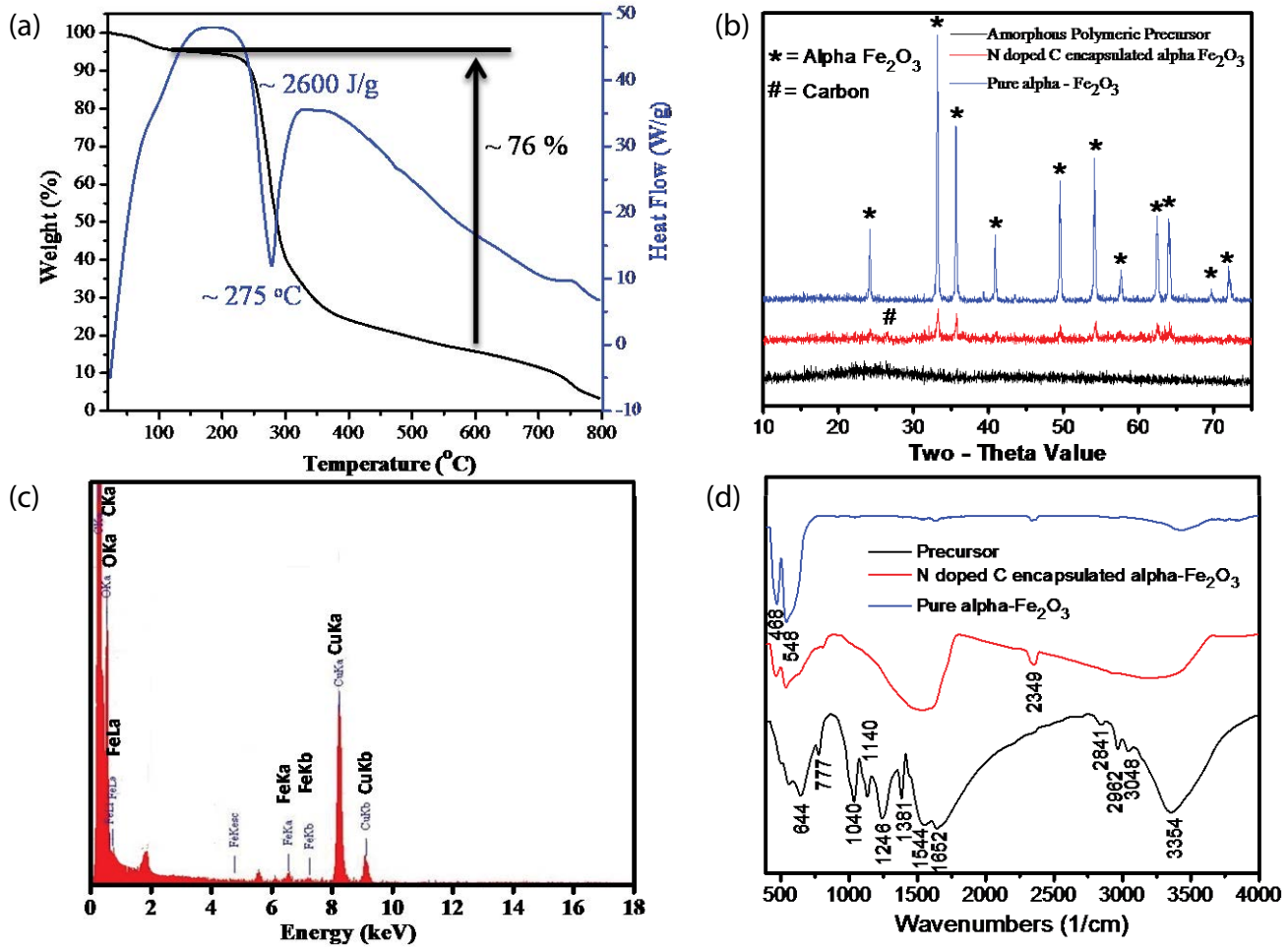

Fig. 1. (a) Thermogravimetric analysis of synthesized polymeric precursor. (b) PXRD of synthesized polymeric precursor, NCF-NC and pure α-Fe_2O_3nanoparticles, (c) EDS analysis of NCF-NC and (d) FTIR spectra of synthesized polymeric precursor, NCF-NC and pure α-Fe_2O_3 nanoparticles.

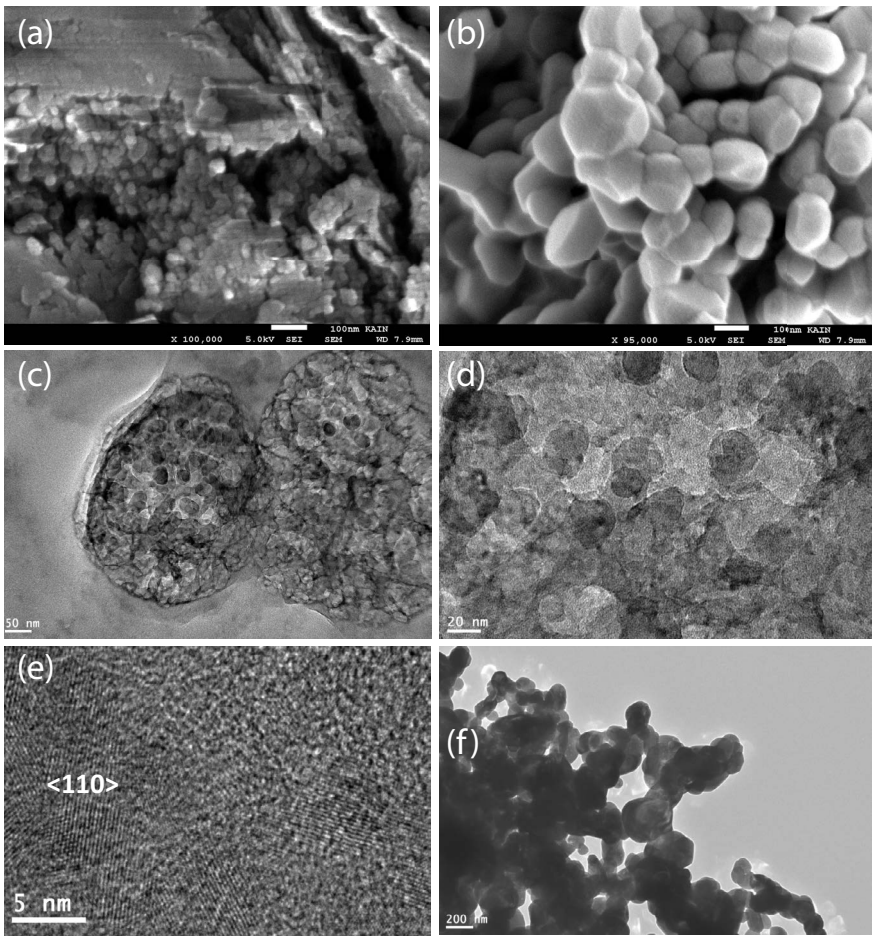

Fig. 2. (a, b) FESEM images of NCF-NC and pure α-Fe_2O_3 nanoparticles, (c,d) FE-TEM, and (e) high-resolution FE-TEM micrographs of NCF-NC, and (d) FE-TEM image of pure α-Fe_2O_3 nanoparticles.

solution phase, which favored the adsorption of H^+ ions instead of Cd^{2+} ions. The adsorption was ~29% at pH 2 and it was increased up to 85% at pH 6. At higher pH, the surface of NCF became negatively charged which assisted the higher adsorption of Cd^{2+} metal ion. After pH 6, there was no significant change in the adsorption percentage. Therefore, pH 6 was chosen as an optimum pH (Fig. 3b). Fig. 3c shows the uptake of Cd^{2+} by NCF at different initial concentrations of Cd^{2+} metal ion. It was observed that the removal of Cd^{2+} was decreased from 87.5% to 58.6% by increasing the concentration of Cd^{2+} from 20 to 100 mg/L which might be due to the saturation of adsorption sites at the higher concentration of Cd^{2+} metal. The adsorption of Cd^{2+} was also influenced by the temperature. It was interesting to note that adsorption was increased with temperature which showed the endothermic nature of adsorption process. The adsorption was raised from 39% to 89% on increasing temperature from 25°C to 40°C (Fig. 3d).

The pseudo-first-order equation is generally expressed as follows:

$$\log\left(q_e - q_t\right) = \log q_e - \frac{k_1 t}{2.303} \tag{2}$$

The pseudo-second-order equation is presented as [46] follows:

$$\frac{t}{q_t} = \frac{1}{k_2 q_e^2} + \frac{1}{q_e} \tag{3}$$

where k_1 (min^{-1}) and k_2 (g/mg min) are the rate constants for pseudo-first order and pseudo-second order reactions, respectively; q_e (mg/g) and q_t (mg/g) are the adsorbed amount of Cd^{2+} metal at equilibrium and at time t, respectively. The values of k_1 and k_2 were calculated using the plots of $\log(q_e - q_t)$ vs. t and t/q_t vs. t, respectively which are shown in Table 1. The correlation coefficients (R^2) values for pseudo-second-order kinetic model were better than that of pseudo-first-order for all the studied concentrations. These findings showed that the current adsorption studies belong to the pseudo-second-order kinetic model well and Cd^{2+} metal was adsorbed on the surface of NCF via chemical interaction such as coordinate or covalent bonds [47] (Fig. 4).

Two frequently used adsorption isotherm models namely Langmuir and Freundlich were used in the present study for data analyses. The Langmuir and Freundlich models are

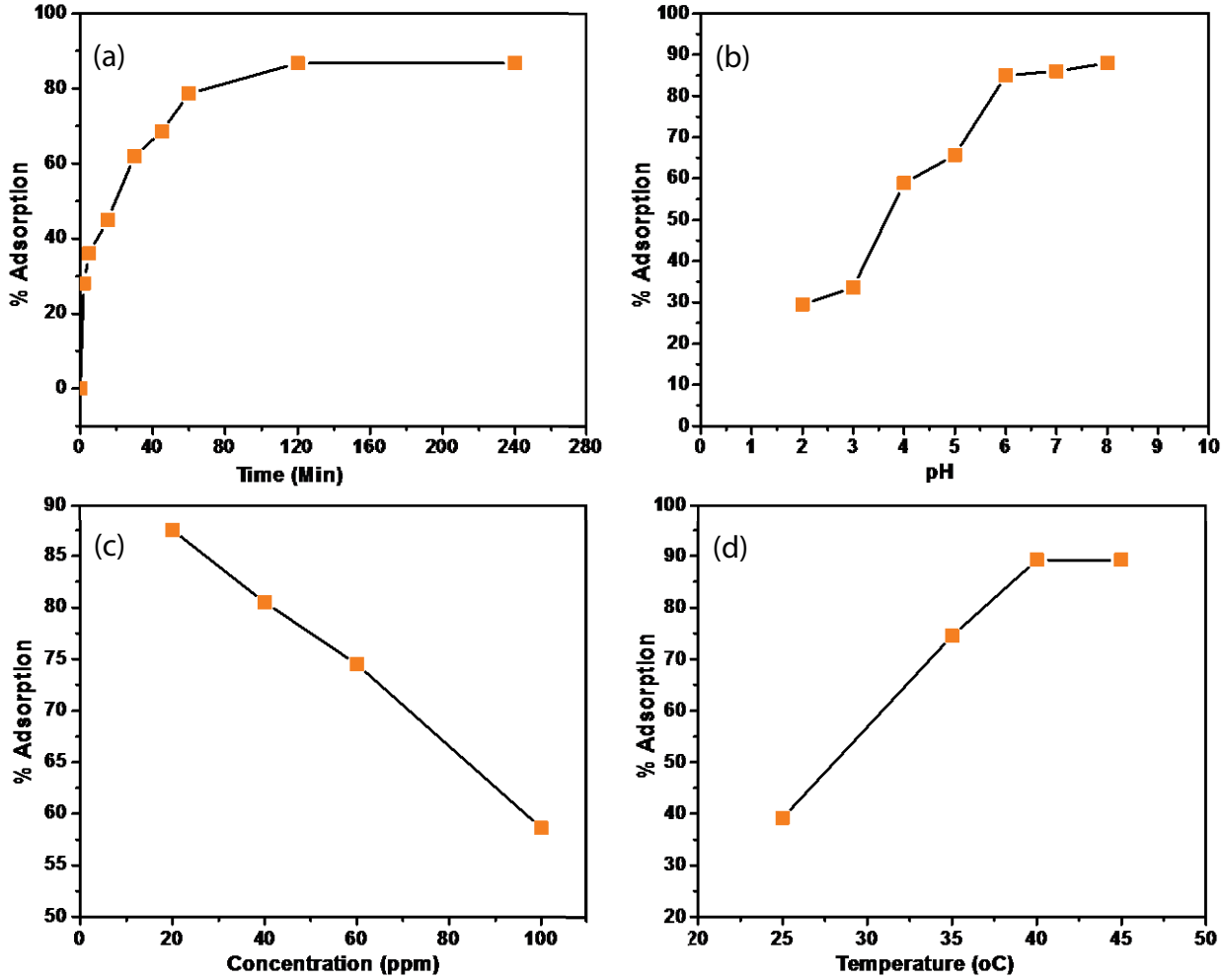

Fig. 3. Removal of Cd^{2+} metal ions using NCF nanocomposite at different (a) time, (b) pH, (c) initial Cd^{2+} concentration, and (d) temperature.

Table 1
Kinetic parameters for the adsorption of Cd^{2+} onto NCF-NC

Kinetic models	Parameters	20 ppm	60 ppm
Pseudo-first-order	q_e (mg g^{-1})	58.9	162
	k_1 (min^{-1})	3.2×10^{-2}	2.7×10^{-2}
	R^2	0.991	0.992
Pseudo-second-order	q_e (mg g^{-1})	81.3	222.2
	k_2 (g mg^{-1} min^{-1})	17.3×10^{-4}	5.73×10^{-4}
	R^2	0.979	0.978

shown in Fig. 5. The Langmuir isotherm model [48] can be represented as:

$$\frac{1}{q_e} = \frac{1}{q_m} + \frac{1}{bq_mC_e} \tag{4}$$

where q_m and b values are calculated from the intercept and slope of linear plots of $1/q_e$ vs. $1/C_e$, respectively and the results are summarized in Table 2. A dimensionless equilibrium parameter (R_L) was evaluated as [49]:

$$R_L = \frac{1}{1+bC_0} \tag{5}$$

In the present study, the values of $R_L < 1$ show the favorable adsorption of Cd^{2+} onto NCF-NC. The linearized form of Freundlich isotherm is given as:

$$\log q_e = \log K_f + \frac{1}{n}\ln C_e \tag{6}$$

K_f and n are Freundlich isotherm constants, which resemble to the adsorption capacity and adsorption intensity, respectively. The values of K_f and n can be calculated from the linear plots of log q_e vs. log C_e. The values of Langmuir and Freundlich parameters are shown in Table 2. The value of n was more than unity at all temperatures which designated a good adsorption process. The value of K_f was increased with temperature which supported an endothermic nature

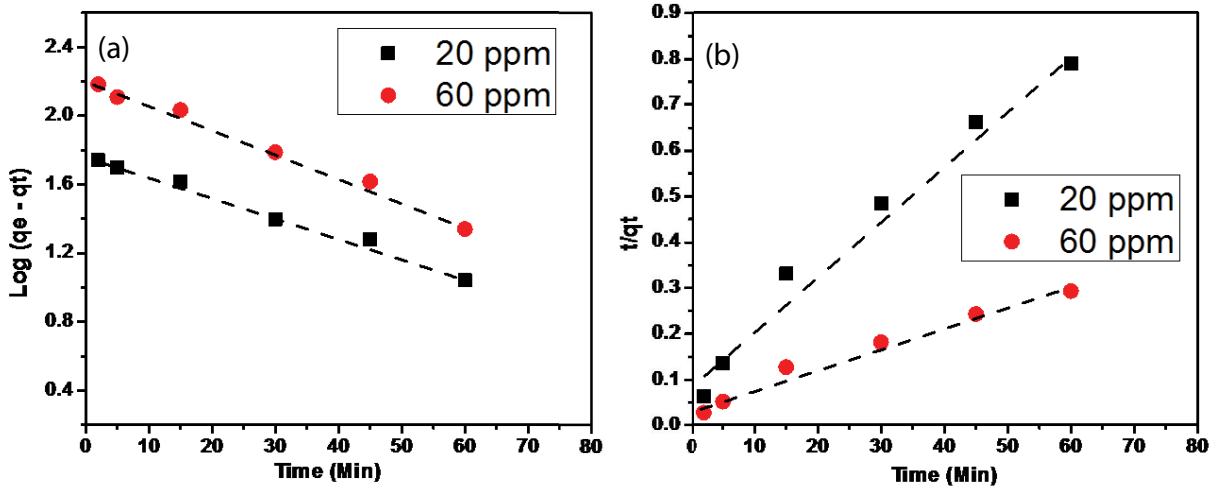

Fig. 4. Plots of kinetic models for the adsorption of Cd^{2+} metal ion using NCF nanocomposite (a) pseudo-first-order and (b) pseudo-second-order models.

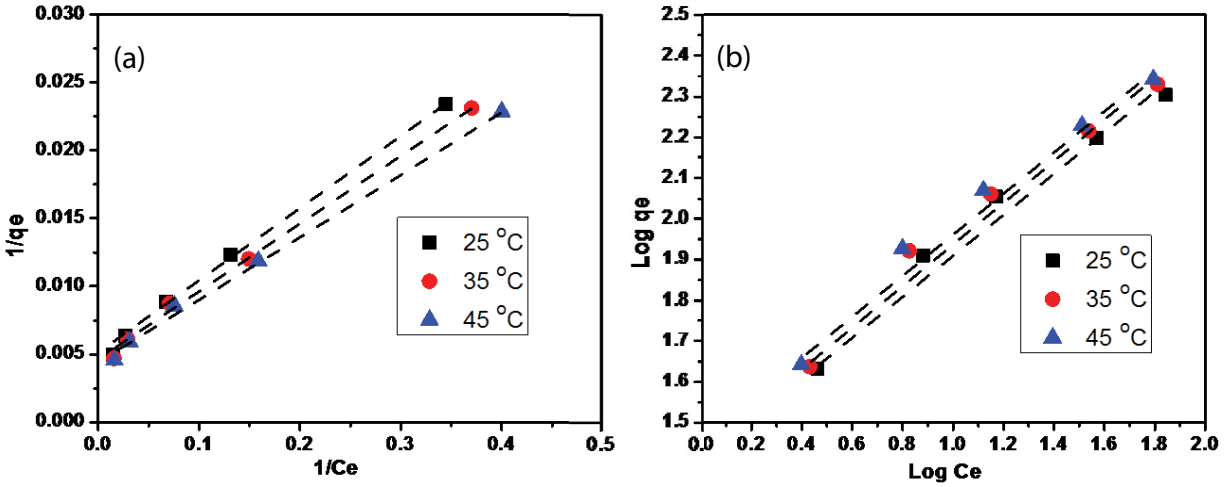

Fig. 5. Plots of isotherm models for the adsorption of Cd(II) using NCF nanocomposite (a) Langmuir isotherm and (b) Freundlich isotherm models.

Table 2
Isotherm model parameters for the adsorption of Cd^{2+} onto NCF-NC

Equilibrium model	Parameters	25°C	35°C	45°C
Langmuir isotherm	q_m (mg g^{-1})	208.3	222.2	227.3
	b (L mg^{-1})	8.72×10^{-2}	8.91×10^{-2}	9.56×10^{-2}
	R_L	0.36	0.35	0.34
	R^2	0.997	0.996	0.996
Freundlich isotherm	K_f (L mg^{-1})	28.5	29.6	31.04
	n	2.11	2.08	2.05
	R^2	0.979	0.980	0.982

of adsorption process. The Langmuir model resulted into a better fit than the Freundlich model as Langmuir isotherm model had higher values of correlation coefficients.

The thermodynamic studies were performed to examine whether the adsorption process spontaneous or non-spontaneous and endothermic or exothermic. Our results showed that the adsorption of Cd(II) was increased with increasing the temperature which proposed an endothermic nature of adsorption. The values of $\Delta H°$ (enthalpy change) and $\Delta S°$ (entropy change) were calculated using the

slopes and intercepts of the plots of ln K_c vs. $1/T$ using the following equation:

$$\ln K_c = -\frac{\Delta H^\circ}{RT} + \frac{\Delta S^\circ}{R} \quad (7)$$

$$\Delta G^\circ = \Delta H^\circ - T\Delta S^\circ \quad (8)$$

The values of all thermodynamic parameter are shown in Table 3. The positive values of ΔH° showed the endothermic adsorption process and the values of ΔH° was >40 kJ mol^{-1}, which suggest the chemical nature of adsorption. The positive values of ΔS° reflect an increment in the randomness at the interface of solid/liquid during the adsorption process. The negative values of ΔG° indicated that the adsorption of Cd(II) onto the NCF-NC was spontaneous process. The adsorption capacity of NCF-NCs was compared with other materials used for the removal of Cd^{2+} metal. The adsorption capacities of NCF material was much higher than other adsorbents listed in Table 4.

Fig. 6 shows the FTIR spectra of NCF-NC before and after adsorption of Cd(II) ions from water. FTIR spectra of NCF-NC show peaks at various frequencies of various functional groups as also discussed above. This study clearly shows that the frequencies of bands are deflected after adsorption, which indicates the involvement of the functional groups in adsorption. A sharp band at ~786 cm^{-1} also appears after adsorption which could be attributed to Cd–O bond [60]. The chemical composition and oxidation state of metal ions were analyzed by XPS technique. Fig. 7a displays the signals corresponding to C1s, N1s, O1s and Fe before adsorption of Cd^{2+}. After adsorption of Cd(II), XPS shows additional peaks of Cd(3d) which supports the adsorption of Cd^{2+} onto the novel adsorbent. XPS spectra of adsorbent (NCF) show two peaks at 710.8 and 724.3 eV with satellites, and they correspond to Fe $2p_{3/2}$ and Fe $2p_{1/2}$ orbits, respectively (Fig. 7b). No any characteristic peaks related with Fe^{2+} ion or Fe metal are noticed, suggesting the Fe species in the adsorbent is in the form of Fe^{3+} ion. The high-resolution XPS spectrum of C 1s illustrated in Fig. 7c which shows four obvious peaks at 284.3, 285.2, 285.8 and 288.6 eV belonging to C–C, C–N, C–O and O–C=O groups, respectively. As shown in Fig. 7d, the peak of N(1s) decomposes into three sub-bands at ~398, ~399 and ~401 eV of pyridinic-type N, pyrrolic-type N and graphitic-type N, respectively, which indicate that nitrogen atoms are successfully doped into

Table 3
Thermodynamics parameters for the adsorption of Cd^{2+} onto NCF-NC (Cd^{2+} concentration 20 and 60 mg L^{-1}; temperature: 298–318 K)

C_0 (mg L^{-1})	ΔH° (kJ mol^{-1})	ΔS° (kJ mol^{-1} K^{-1})	$-\Delta G^\circ$ (kJ mol^{-1})		
			298 K	308 K	318 K
20	43.28	0.16	3.80	5.38	6.96
60	41.25	0.15	3.15	4.64	6.87

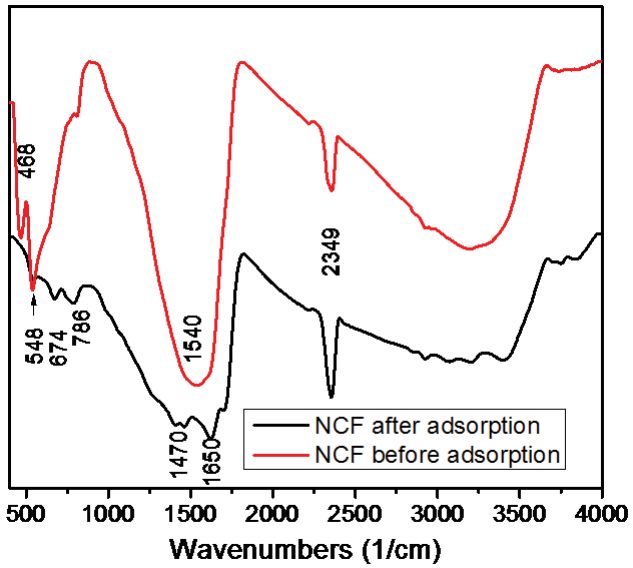

Fig. 6. FTIR spectra of NCF-NC before and after adsorption of Cd(II) ions.

Table 4
Comparison of the adsorption capacity of NCF-NC with reported adsorption capacities of other adsorbents

Adsorbent	Adsorption isotherms	Q_{max} (mg/g)	References
β-CD polymer	Freundlich	163.2	[50]
Activated carbon	Freundlich	15.7	[51]
Biochars	Freundlich	13.2	[52]
Graphene	Langmuir	57.6	[53]
Plantain peels	Langmuir	70.9	[54]
TBA-kaolinite	Langmuir and Freundlich	9.8	[55]
Saw dust	Langmuir	5.4	[56]
MnO_2-loaded resin	Langmuir	21.5	[57]
Glebionis coronaria L. activated carbon	Langmuir	115.9	[58]
Bamboo charcoal	Langmuir	12.1	[59]
NCF	Langmuir	208.3	Present study

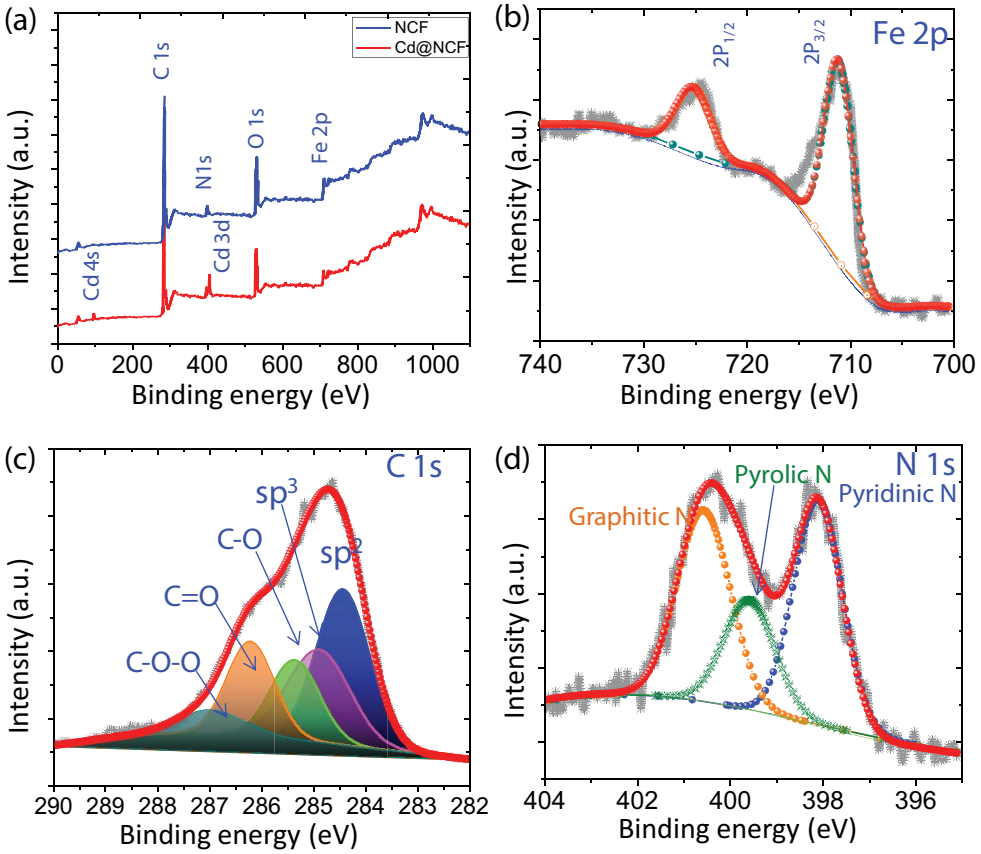

Fig. 7. (a) XPS spectra of NCF-NC before (blue colored line) and after (red colored line) adsorption of cadmium(II). High-resolution XPS spectra of NCF-NC containing (b) Fe2p, (c) C1s, and (d) N1s.

carbon matrix. The O1s spectrum can be deconvoluted into three peak sets, C=O bond at 532.6 eV, C–O bond at 530.6 eV and O^{2-} at 529.9 eV.

4. Conclusions

Nitrogen-doped carbon-encapsulated α-Fe_2O_3 (NCF) nanocomposites have been synthesized at 325°C and used as efficient adsorbent materials in wastewater treatment for removal of Cd(II) ion. Encapsulated α-Fe_2O_3 nanoparticles in nitrogen-doped carbon were clearly observed by electron microscopy, FTIR and XPS studies. Batch adsorption studies were also performed and optimized under various adsorption parameters. XPS analysis was carried out before and after adsorption of heavy metals. The adsorption of Cd^{2+} onto the NCF-NC was an endothermic process. The enhanced adsorption capacity of NCF-NC was found to be ~208.3 mg/g at 25°C using the Langmuir equation. Present study showed that NCF-NCs are promising adsorbent materials for treating Cd-bearing wastewater.

Acknowledgment

The authors extend their sincere appreciation to the Deanship of Scientific Research at King Saud University for funding this Research Group (RG-1439-87).

Conflict of interest

The authors declare that they have no conflict of interest.

References

[1] J. Gong, T. Liu, X. Wang, X. Hu, L. Zhang, Efficient removal of heavy metal ions from aqueous systems with the assembly of anisotropic layered double hydroxide nanocrystals@carbon nanosphere, Environ. Sci. Technol., 45 (2011) 6181–6187.
[2] X.-j. Hu, J.-s. Wang, Y.-g. Liu, X. Li, G.-m. Zeng, Z.-l. Bao, X.-x. Zeng, A.-w. Chen, F. Long, Adsorption of chromium (VI) by ethylenediamine-modified cross-linked magnetic chitosan resin: isotherms, kinetics and thermodynamics, J. Hazard. Mater., 185 (2011) 306–314.
[3] T. Ahamad, M. Naushad, B.M. Al-Maswari, J. Ahmed, Z.A. Alothman, S.M. Alshehri, A.A. Alqadami, Synthesis of a recyclable mesoporous nanocomposite for efficient removal of toxic Hg^{2+} from aqueous medium, J. Ind. Eng. Chem., 53 (2017) 268–275.
[4] X. Qu, P.J.J. Alvarez, Q. Li, Applications of nanotechnology in water and wastewater treatment, Water Res., 47 (2013) 3931–3946.
[5] M. Naushad, A. Mittal, M. Rathore, V. Gupta, Ion-exchange kinetic studies for Cd(II), Co(II), Cu(II), and Pb(II) metal ions over a composite cation exchanger, Desal. Wat. Treat., 54 (2015) 2883–2890.
[6] M. Naushad, Z.A. Alothman, Separation of toxic Pb^{2+} metal from aqueous solution using strongly acidic cation-exchange resin: analytical applications for the removal of metal ions from pharmaceutical formulation, Desal. Wat. Treat., 53 (2015) 2158–2166.

[7] P. Grimshaw, J.M. Calo, G. Hradil, Cyclic electrowinning/precipitation (CEP) system for the removal of heavy metal mixtures from aqueous solutions, Chem. Eng. J., 175 (2011) 103–109.
[8] H. Bessbousse, T. Rhlalou, J.-F. Verchère, L. Lebrun, Removal of heavy metal ions from aqueous solutions by filtration with a novel complexing membrane containing poly(ethyleneimine) in a poly(vinyl alcohol) matrix, J. Membr. Sci., 307 (2008) 249–259.
[9] S.M. AlShehri, J. Ahmed, T. Ahamad, B.M. Almaswari, A. Khan, Efficient photodegradation of methylthioninium chloride dye in aqueous using barium tungstate nanoparticles, J. Nanopart. Res., 19 (2017) 289.
[10] T. Ahmad, R. Phul, P. Alam, I.H. Lone, M. Shahazad, J. Ahmed, T. Ahamad, S.M. Alshehri, Dielectric, optical and enhanced photocatalytic properties of $CuCrO_2$ nanoparticles, RSC Adv., 7 (2017) 27549–27557.
[11] B.C. Ricci, C.D. Ferreira, A.O. Aguiar, M.C.S. Amaral, Integration of nanofiltration and reverse osmosis for metal separation and sulfuric acid recovery from gold mining effluent, Sep. Purif. Technol., 154 (2015) 11–21.
[12] M. Naushad, S. Vasudevan, G. Sharma, A. Kumar, Z.A. Alothman, Adsorption kinetics, isotherms, and thermodynamic studies for Hg^{2+} adsorption from aqueous medium using alizarin red-S-loaded amberlite IRA-400 resin, Desal. Wat. Treat., 57 (2016) 18551–18559.
[13] A. Mittal, M. Naushad, G. Sharma, Z.A. ALothman, S.M. Wabaidur, M. Alam, Fabrication of MWCNTs/ThO_2 nanocomposite and its adsorption behavior for the removal of Pb(II) metal from aqueous medium, Desal. Wat. Treat., 57 (2016) 21863–21869.
[14] M. Naushad, Surfactant assisted nano-composite cation exchanger: Development, characterization and applications for the removal of toxic Pb^{2+} from aqueous medium, Chem. Eng. J., 235 (2014) 100–108.
[15] M. Sajid, M.K. Nazal, Ihsanullah, N. Baig, A.M. Osman, Removal of heavy metals and organic pollutants from water using dendritic polymers based adsorbents: a critical review, Sep. Purif. Technol., 191 (2018) 400–423.
[16] Y. Feng, Y. Wang, Y. Wang, S. Liu, J. Jiang, C. Cao, J. Yao, Simple fabrication of easy handling millimeter-sized porous attapulgite/polymer beads for heavy metal removal, J. Colloid Interface Sci., 502 (2017) 52–58.
[17] H. Xiyili, S. Çetintaş, D. Bingöl, Removal of some heavy metals onto mechanically activated fly ash: Modeling approach for optimization, isotherms, kinetics and thermodynamics, Process Saf. Environ. Prot., 109 (2017) 288–300.
[18] A.A. Alqadami, M. Naushad, M.A. Abdalla, T. Ahamad, Z. Abdullah Alothman, S.M. Alshehri, A.A. Ghfar, Efficient removal of toxic metal ions from wastewater using a recyclable nanocomposite: a study of adsorption parameters and interaction mechanism, J. Cleaner Prod., 156 (2017) 426–436.
[19] S. Gokila, T. Gomathi, P.N. Sudha, S. Anil, Removal of the heavy metal ion chromiuim(VI) using chitosan and alginate nanocomposites, Int. J. Biol. Macromol., 104 (2017) 1459–1468.
[20] M.E. Mahmoud, A.E.H. Abdou, M.E. Sobhy, N.A. Fekry, Solid–solid crosslinking of carboxymethyl cellulose nanolayer on titanium oxide nanoparticles as a novel biocomposite for efficient removal of toxic heavy metals from water, Int. J. Biol. Macromol., 105 (2017) 1269–1278.
[21] A.A. Alqadami, M. Naushad, Z.A. Alothman, A.A. Ghfar, Novel metal–organic framework (MOF) Based composite material for the sequestration of U(VI) and Th(IV) metal ions from aqueous environment, ACS Appl. Mater. Interfaces, 9 (2017) 36026–36037.
[22] G. Sharma, M. Naushad, A. Kumar, S. Rana, S. Sharma, A. Bhatnagar, F.J. Stadler, A.A. Ghfar, M.R. Khan, Efficient removal of coomassie brilliant blue R-250 dye using starch/poly(alginic acid-cl-acrylamide) nanohydrogel, Process Saf. Environ. Prot., 109 (2017) 301–310.
[23] S. Lin, C. Lian, M. Xu, W. Zhang, L. Liu, K. Lin, Study on competitive adsorption mechanism among oxyacid-type heavy metals in co-existing system: removal of aqueous As(V), Cr(III) and As(III) using magnetic iron oxide nanoparticles (MIONPs) as adsorbents, Appl. Surf. Sci., 422 (2017) 675–681.
[24] C. Santhosh, R. Nivetha, P. Kollu, V. Srivastava, M. Sillanpää, A.N. Grace, A. Bhatnagar, Removal of cationic and anionic heavy metals from water by 1D and 2D-carbon structures decorated with magnetic nanoparticles, Sci. Rep., 7 (2017) 14107.
[25] S. Jin, B.C. Park, W.S. Ham, L. Pan, Y.K. Kim, Effect of the magnetic core size of amino-functionalized Fe_3O_4-mesoporous SiO_2 core-shell nanoparticles on the removal of heavy metal ions, Colloids Surf., A, 531 (2017) 133–140.
[26] H. Yang, Y. Chen, Q. Feng, H. Tian, J. Li, Preparation of ion-imprinted amino-functionalized nano-porous silica for selective removal of heavy metal ions from water environment, J. Nanosci. Nanotechnol., 17 (2017) 6818–6826.
[27] M. Naushad, T. Ahamad, G. Sharma, A.H. Al-Muhtaseb, A.B. Albadarin, M.M. Alam, Z.A. ALOthman, S.M. Alshehri, A.A. Ghfar, Synthesis and characterization of a new starch/SnO_2 nanocomposite for efficient adsorption of toxic Hg^{2+} metal ion, Chem. Eng. J., 300 (2016) 306–316
[28] H.I. Maarof, M.A. Ajeel, W.M.A.W. Daud, M.K. Aroua, Electrochemical properties and electrode reversibility studies of palm shell activated carbon for heavy metal removal, Electrochim. Acta, 249 (2017) 96–103.
[29] H. Tounsadi, A. Khalidi, A. Machrouhi, M. Farnane, R. Elmoubarki, A. Elhalil, M. Sadiq, N. Barka, Highly efficient activated carbon from Glebionis coronaria L. biomass: optimization of preparation conditions and heavy metals removal using experimental design approach, J. Environ. Chem. Eng., 4 (2016) 4549–4564.
[30] P.S. Thue, E.C. Lima, J.M. Sieliechi, C. Saucier, S.L.P. Dias, J.C.P. Vaghetti, F.S. Rodembusch, F.A. Pavan, Effects of first-row transition metals and impregnation ratios on the physicochemical properties of microwave-assisted activated carbons from wood biomass, J. Colloid Interface Sci., 486 (2017) 163–175.
[31] Z. Liu, F. Zhang, T. Liu, N. Peng, C. Gai, Removal of azo dye by a highly graphitized and heteroatom doped carbon derived from fish waste: adsorption equilibrium and kinetics, J. Environ. Manage., 182 (2016) 446–454.
[32] H.-J. Cui, J.-K. Cai, J.-W. Shi, B. Yuan, C.-L. Ai, M.-L. Fu, Fabrication of 3D porous Mn doped α-Fe_2O_3 nanostructures for the removal of heavy metals from wastewater, RSC Adv., 4 (2014) 10176–10179.
[33] A. Mahapatra, B.G. Mishra, G. Hota, Electrospun Fe_2O_3–Al_2O_3 nanocomposite fibers as efficient adsorbent for removal of heavy metal ions from aqueous solution, J. Hazard. Mater., 258–259 (2013) 116–123.
[34] R. Ravindranath, P. Roy, A.P. Periasamy, Y.-W. Chen, C.-T. Liang, H.-T. Chang, Fe_2O_3/Al_2O_3 microboxes for efficient removal of heavy metal ions, New J. Chem., 41 (2017) 7751–7757.
[35] X. Yang, X. Wang, Y. Feng, G. Zhang, T. Wang, W. Song, C. Shu, L. Jiang, C. Wang, Removal of multifold heavy metal contaminations in drinking water by porous magnetic Fe_2O_3@AlO(OH) superstructure, J. Mater. Chem. A, 1 (2013) 473–477.
[36] T.A. Khan, S.A. Chaudhry, I. Ali, Equilibrium uptake, isotherm and kinetic studies of Cd(II) adsorption onto iron oxide activated red mud from aqueous solution, J. Mol. Liq., 202 (2015) 165–175.
[37] H.-J. Cui, J.-K. Cai, H. Zhao, B. Yuan, C. Ai, M.-L. Fu, One step solvothermal synthesis of functional hybrid γ-Fe_2O_3/carbon hollow spheres with superior capacities for heavy metal removal, J. Colloid Interface Sci., 425 (2014) 131–135.
[38] S.M. AlShehri, J. Ahmed, A.M. Alzahrani, T. Ahamad, Synthesis, characterization, and enhanced photocatalytic properties of $NiWO_4$ nanobricks, New J. Chem., 41 (2017) 8178–8186.
[39] S. Hajati, S. Tougaard, J. Walton, N. Fairley, Noise reduction procedures applied to XPS imaging of depth distribution of atoms on the nanoscale, Surf. Sci., 602 (2008) 3064–3070.
[40] S. Hajati, S. Coultas, C. Blomfield, S. Tougaard, XPS imaging of depth profiles and amount of substance based on Tougaard's algorithm, Surf. Sci., 600 (2006) 3015–3021.
[41] J. Ahmed, T. Ahmad, K.V. Ramanujachary, S.E. Lofland, A.K. Ganguli, Development of a microemulsion-based process

for synthesis of cobalt (Co) and cobalt oxide (Co_3O_4) nanoparticles from submicrometer rods of cobalt oxalate, J. Colloid Interface Sci., 321 (2008) 434–441.
[42] B. Ramesh Babu, S. Vahidhabanu, A. Abideen Idowu, Magnetic core layered double hydroxide over halloysite as a robust adsorbent for the treatment of dye-contaminated wastewater: a clean approach for industrial applications, Desal. Wat. Treat., 138 (2019) 379–388.
[43] S. Vahidhabanu, A. Abideen Idowu, D. Karuppasamy, B. Ramesh Babu, M. Vineetha, Microwave initiated facile formation of sepiolite-poly (dimethylsiloxane) nanohybrid for effective removal of Congo red dye from aqueous solution, ACS Sustainable Chem. Eng., 5 (2017) 10361–10370.
[44] Z.A. AL-Othman, R. Ali, M. Naushad, Hexavalent chromium removal from aqueous medium by activated carbon prepared from peanut shell: adsorption kinetics, equilibrium and thermodynamic studies, Chem. Eng. J., 184 (2012) 238–247.
[45] S.M. Alshehri, M. Naushad, T. Ahamad, Z.A. Alothman, A. Aldalbahi, Synthesis, characterization of curcumin based ecofriendly antimicrobial bio-adsorbent for the removal of phenol from aqueous medium, Chem. Eng. J., 254 (2014) 181–189.
[46] Y.S. Ho, G. McKay, D.A.J. Wase, C.F. Forster, Study of the sorption of divalent metal ions on to peat, Adsorpt. Sci. Technol., 18 (2000) 639–650.
[47] A.A. Attia, S.A. Khedr, S.A. Elkholy, Adsorption of chromium ion (VI) by acid activated carbon, Braz. J. Chem. Eng., 27 (2010) 183–193.
[48] I. Langmuir, The adsorption of gases on plane surfaces of glass, mica and platinum, J. Am. Chem. Soc., 40 (1918) 1361–1403.
[49] M. Naushad, T. Ahamad, B.M. Al-Maswari, A. Abdullah Alqadami, S.M. Alshehri, Nickel ferrite bearing nitrogen-doped mesoporous carbon as efficient adsorbent for the removal of highly toxic metal ion from aqueous medium, Chem. Eng. J., 330 (2017) 1351–1360.
[50] J. He, Y. Li, C. Wang, K. Zhang, D. Lin, L. Kong, J. Liu, Rapid adsorption of Pb, Cu and Cd from aqueous solutions by β-cyclodextrin polymers, Appl. Surf. Sci., 426 (2017) 29–39.
[51] M.M. Rao, D.K. Ramana, K. Seshaiah, M.C. Wang, S.W.C. Chien, Removal of some metal ions by activated carbon prepared from Phaseolus aureus hulls, J. Hazard. Mater., 166 (2009) 1006–1013.
[52] W.-K. Kim, T. Shim, Y.-S. Kim, S. Hyun, C. Ryu, Y.-K. Park, J. Jung, Characterization of cadmium removal from aqueous solution by biochar produced from a giant Miscanthus at different pyrolytic temperatures, Bioresour. Technol., 138 (2013) 266–270.
[53] Y. Shen, B. Chen, Sulfonated Graphene Nanosheets as a superb adsorbent for various environmental pollutants in water, Environ. Sci. Technol., 49 (2015) 7364–7372.
[54] Z.N. Garba, N.I. Ugbaga, A.K. Abdullahi, Evaluation of optimum adsorption conditions for Ni (II) and Cd (II) removal from aqueous solution by modified plantain peels (MPP), Beni-Suef Univ. J. Basic Appl. Sci., 5 (2016) 170–179.
[55] S.S. Gupta, K.G. Bhattacharyya, Removal of Cd(II) from aqueous solution by kaolinite, montmorillonite and their poly(oxo zirconium) and tetrabutylammonium derivatives, J. Hazard. Mater., 128 (2006) 247–257.
[56] Y. Bulut, Z. Tez, Removal of heavy metals from aqueous solution by sawdust adsorption, J. Environ. Sci., 19 (2007) 160–166.
[57] L. Dong, Z. Zhu, H. Ma, Y. Qiu, J. Zhao, Simultaneous adsorption of lead and cadmium on MnO_2-loaded resin, J. Environ. Sci., 22 (2010) 225–229.
[58] H. Tounsadi, A. Khalidi, M. Farnane, M. Abdennouri, N. Barka, Experimental design for the optimization of preparation conditions of highly efficient activated carbon from Glebionis coronaria L. and heavy metals removal ability, Process Saf. Environ. Prot., 102 (2016) 710–723.
[59] F.Y. Wang, H. Wang, J.W. Ma, Adsorption of cadmium (II) ions from aqueous solution by a new low-cost adsorbent—Bamboo charcoal, J. Hazard. Mater., 177 (2010) 300–306.
[60] P.V. Dalal, Nucleation Controlled growth of cadmium oxalate crystals in agar gel and their characterization, Indian J. Mater. Sci., 2013 (2013) 1–5.